TECHNICAL MEMORANDUMS

NATIONAL ADVISORY COMMITTEE FOR AERONAUTICS

NACA-TM-856

No. 856

THE LIFT DISTRIBUTION OF WINGS WITH END PLATES

By W. Mangler

Luftfahrtforschung
Vol. 14, No. 11, November 20, 1937
Verlag von R. Oldenbourg, München und Berlin

Washington
April 1938

NATIONAL ADVISORY COMMITTEE FOR AERONAUTICS

TECHNICAL MEMORANDUM NO. 856

THE LIFT DISTRIBUTION OF WINGS WITH END PLATES*

By W. Mangler

SUMMARY

This report describes the lift distribution on wings with end plates for the case of minimum induced drag (induced downwash constant over the span). The moments on the end plates are also determined.

It is found that moving an end plate of certain length up from the symmetrical position, is followed by a slight increase of the total lift. As a marked increase in the moments of the end plate about its attachment also results, the symmetrical end plates are most advantageous if a higher circulation on the wing only is contemplated. But, if the end plates are to serve for producing horizontal control forces, a pronounced unsymmetrical arrangement will be preferred.

The magnitude of the ensuing side force for end plates of any length and position is illustrated in figure 13. The ratio of coefficients of side force and of lift can be interpolated from figure 14. For the application of the side force, an empirical formula (22) is given.

The writer wishes to express his appreciation to Miss I. Lotz, for the many suggestions in the preparation of the study.

NOTATION

b, wing span.

h, height of end plate.

k_o, ratio of height of the upper part of the end plate to semispan.

---

*"Die Auftriebsverteilung am Tragflügel mit Endscheiben." Luftfahrtforschung, vol. 14, no. 11, November 20, 1937, pp. 564-569.

NOTATION (Cont.)

k_u, ratio of height of the lower part of the end plate to $b/2$.

$k = \frac{k_o}{k_u}$, ratio of height of upper to height of lower part of the end plate ($k = 1$ for symmetrical end plates).

$\frac{h}{b} = \frac{k_o + k_u}{2}$, ratio of height of end plate to span.

$\bar{\xi}$, coordinate (referred to $\frac{b}{2} = 1$) along the span.

$\bar{\eta}$, coordinate (referred to $\frac{b}{2} = 1$) along the end plate.

$\zeta = \xi + i\eta$, coordinates in a plane through the vortex surface shed by the wing (referred to $b/2 = 1$).

Γ, circulation.

A, lift.

c_a, lift coefficient.

W_i, induced drag.

c_{w_i}, drag coefficient.

w_i, rate of downwash induced by the vortices leaving the wing.

$2w_i = w$ rate of downwash induced by the vortices at great distance behind the wing.

V, air speed.

ρ, air density.

$q = \frac{\rho}{2} V^2$, dynamic pressure.

$F = b\ t$, wing area.

S_o (or S_u), side force on upper (or lower) part of the end plate.

NOTATION (Cont.)

F_o (or F_u), area of upper (or lower) part of end plate.

c_{s_o} (or c_{s_u}), side force coefficient referred to F_o (or F_u).

M_o (or M_u), moment exerted by S_o (or S_u) about the point of attachment of the plate.

I. INTRODUCTION

Wings with end plates (fig. 1) are used on sailplanes and lately, also, on the tails of airplanes.

The object of the present report is to ascertain the relationship of the circulation distribution over the wing and of the lift to the height and position of the end plate. The side forces and moments on the end plates were also determined.

The investigation hereinafter treats the case of minimum induced drag, i.e., the case where the rate of downwash w_i induced at the wing by the shedding vortices is constant over the span, and where the shedding vortex surface moves downward at a constant rate $2w_i = w$ like a solid body (references 1 and 2).

The case of symmetrical end plates ($k = 1$) was treated according to F. Nagel (reference 3). For small, one-sided end plates ($k = \infty$). I also had access to the unpublished calculations by F. Keune.

II. LIFT AND MOMENTS

Assume a plane placed at right angles to the stream direction through the shedding vortex surface at a great distance behind the wing. Provided that the downward velocity of the vortex surface (which has the value of $w = 2w_i$ if w_i is the downward velocity created by the vortices at the wing) is small- that is, no rolling up of the vortex surface takes place - this section has the form indicated in figure 2. Our problem can then be solved if we

treat the plane problem of the flow around the section of figure 2, through the vortex layer. To make the problem steady, it may be assumed that the section which is at rest is approached from below at the constant speed $w = 2w_i$.

If the complex potential $[] = \Phi + i\psi$ of this flow is known, the circulation strength at a point $\bar{\xi}$ of the wing or point $\bar{\eta}$ of the end plate (fig. 1), is equal to the jump suffered by the potential when changing at point ξ, corresponding to point $\bar{\xi}$ or point $1 + i\eta$, corresponding to $\bar{\eta}$, respectively, from one side of the vortex layer to the other (figs. 1 and 2). The section being a streamline (reference 4), ψ is constant.

Thus, we have:

$$\left.\begin{aligned} \Gamma(\bar{\xi}) &= \Phi_2(\xi) - \Phi_1(\xi) \\ \Gamma(\bar{\eta}) &= \Phi_2(1 + i\eta) - \Phi_1(1 + i\eta) \end{aligned}\right\} \qquad (1)$$

where Φ_1 and Φ_2 are the potential values for point ξ or $1 + i\eta$).

Then the lift becomes:

$$A = c_a \frac{\rho}{2} V^2 F = \rho V \frac{b}{2} \int_{-1}^{+1} \Gamma(\bar{\xi})\, d\bar{\xi} \qquad (2)$$

With this

$$c_a = \frac{b}{VF} \int_{-1}^{+1} \Gamma(\bar{\xi})\, d\bar{\xi}$$

or, making Γ dimensionless with $w \frac{b}{2}$:

$$c_a = \frac{w}{2V} \frac{b^2}{F} \int_{-1}^{+1} \frac{\Gamma(\bar{\xi})}{w \frac{b}{2}}\, d\bar{\xi}$$

The induced angle of attack α_i becomes:

$$\alpha_i \approx \tan \alpha_i = \frac{w_i}{V} = \frac{w}{2V} = \frac{W_i}{A} = \frac{c_{w_i}}{c_a} \tag{3}$$

which with

$$J = \int_0^1 \frac{\Gamma(\bar{\xi})}{w \frac{b}{2}} \, d\bar{\xi} \tag{4}$$

gives the drag coefficient

$$c_{w_i} = c_a^2 \frac{F}{\pi b^2} \frac{\pi}{2J} = c_a^2 \frac{F}{\pi b^2} \kappa \tag{5}$$

In this form the factor $\kappa = \frac{\pi}{2J}$ gives at once the departure of the drag coefficient from that of the elliptical wing. For equal lift and dynamic pressure a wing of span b with end plates has the same induced drag as a wing of $\frac{b}{\sqrt{\kappa}}$ span without end plates.

For the determination of the side forces and moments at the end plate, the sense of rotation of the bound and free vortices is given in figure 3. Seen from above, the bound vortices of the right-hand end plate turn in the upper part in positive direction; in the lower part, in negative direction; so that the air speed V causes a force perpendicular to V and to the end plate. In the upper part this force is inwardly, in the lower part outwardly, directed. The forces created by the right and left end plates cancel each other, but exert a moment about the point of attachment of the end plates.

For the side force S_o, in the upper part of the end plate, we have:

$$S_o = \rho V \frac{b}{2} \int_0^{k_o} \Gamma(\bar{\eta}) \, d\bar{\eta} \tag{6}$$

where

$$k_o = \frac{k}{1 + k} \frac{2h}{b}$$

We write:

$$J_o = \int_o^{k_o} \frac{\Gamma(\bar{\eta})}{w \frac{b}{2}} \, d\bar{\eta} \tag{7}$$

and find from equations (2) and (6) in conjunction with equation (4), the ratio of side force to lift at:

$$\frac{S_o}{A} = \frac{J_o}{2J} \tag{8}$$

and correspondingly for the lower part:

$$\frac{S_u}{A} = \frac{J_u}{2J} \tag{9}$$

where

$$J_u = \int_{-k_u}^{o} \frac{\Gamma(\bar{\eta})}{w \frac{b}{2}} \, d\bar{\eta}$$

and

$$k_u = \frac{1}{1 + k} \frac{2h}{b}$$

The side force coefficient c_{s_o} is introduced through the relation

$$S_o = c_{s_o} \frac{\rho}{2} V^2 F_o$$

where F_o denotes the area of the upper part of the end plate.

Assuming the wing to be rectangular ($F = b\ t$) with elliptical end plates

$$\left(F_o = \frac{\pi}{8} k_o\ b\ t; \quad F_u = \frac{\pi}{8} k_u\ b\ t\right)$$

we find:

$$\frac{c_{s_o}}{c_a} = \frac{J_o}{2J} \frac{F}{F_o} = \frac{J_o}{2J} \frac{8}{\pi} \frac{1}{k_o} \tag{8a}$$

and

$$\frac{c_{s_u}}{c_a} = \frac{J_u}{2J}\frac{F}{F_u} = \frac{J_u}{2J}\,\frac{8}{\pi}\,\frac{1}{k_u} \tag{9a}$$

The moment M_o of the side force S_o, is given by

$$M_o = \rho\, V\, \frac{b^2}{4} \int_0^{k_o} \Gamma(\bar{\eta})\, \bar{\eta}\, d\bar{\eta} \tag{10}$$

With equations (3) and (5) the moment about the upper part of the end plate becomes:

$$\frac{M_o}{A\,\frac{b}{2}} = \frac{J_o{}^*}{2J} \tag{11}$$

and about the lower part:

$$\frac{M_u}{A\,\frac{b}{2}} = \frac{J_u{}^*}{2J} \tag{12}$$

if we put:

$$\left.\begin{aligned} J_o{}^* &= \int_0^{k_o} \frac{\Gamma(\bar{\eta})}{w\,\frac{b}{2}}\, \bar{\eta}\, d\bar{\eta} \\ \text{and} \qquad J_u{}^* &= \int_{-k_u}^{0} \frac{\Gamma(\bar{\eta})}{w\,\frac{b}{2}}\, \bar{\eta}\, d\bar{\eta} \end{aligned}\right\} \tag{13}$$

Finally, equations (10), (8), and (11) yield for the lever arm at the upper part of the plate, the formula:

$$\eta_o = \frac{M_o}{\left(\frac{b}{2}\right) S_o} = \frac{M_o}{A\,\frac{b}{2}}\,\frac{A}{S_o} = \frac{J_o{}^*}{J_o} \tag{14}$$

and at the lower part:

$$\eta_u = \frac{J_u{}^*}{J_u} \tag{15}$$

III. TRANSFORMATION

The flow potential $\square|\square\ (\zeta)$ in the (ξ, η) plane is determined by so transforming the (ξ, η) plane through an analytical function $\zeta = f(z)$ into the z plane $(z = x + iy)$ that the right ζ half plane $(\xi > 0)$ is transformed into the upper z-half plane $(y > 0)$ at the same time as the right-hand part of the section and the imaginary ζ-axis changes into the real z-axis (fig. 4). Then the flow potential $\square|\square\ (z)$ and consequently, also, $\square|\square\ (\zeta)$ can be readily established.

The desired transformation could be easily expressed with the Schwarz-Christoffel transformation formula, which would give an elliptical integral whose parameters - the points of the z-plane for the corners of the ζ-plane, would have to be determined through the geometrical quantities of the ζ-plane. But as this would entail the solution of a system of five transcendent equations with five unknown quantities, a different way, an approximate method, is preferable. The desired transformation is built up in three stages:

1st stage: $$\zeta = + \sqrt{z'} \tag{16}$$

The half plane $\xi > 0$, to which we can confine ourselves for reasons of symmetry, goes into the z'-plane (figs. 5 and 6).

The straight pieces BC and ED become the parabolic arcs B'C' and E'D'. It is permissible to assume that the ratio k of the distances BC and ED is $\geqq 1$: $k = \frac{k_o}{k_u} \geqq 1$. In addition, since we treat only the cases where $k_o \leqq 1$ (i.e., the upper end plate piece is less than half the span), the parabolic arc C'B'E'D' may be substituted by a circle.

This circle is to be so chosen that its center lies on the real axis and passes through B' and C'. Its equation reads:

$$x'^2 - 2ax' + y'^2 = 1 - 2a$$

whereby the center lies at the point $a = -(1 + \frac{1}{2} k_o^2)$.

It also intersects the real axis in the point $G' = L' = -(3 + k_o^2)$ (fig. 6).

Now every point of the parabola is projected parallel to axis y' on the circle. (Any other projection would serve as well; we chose the most convenient one.) This means that the investigation tends toward end plates with small outward curvature rather than flat ones. This curvature, which depends on h/b, is negligibly small in our case.

Point $D' = (1 - k_u^2) - 2i\,k_u$

is replaced by

$$D'_1 = (1 - k_u^2) - 2i\,k_u \sqrt{1 + \frac{1}{4}(k_o^2 - k_u^2)}$$

2d stage: $$z' = \frac{(3 + k_o^2)\,z''}{(4 + k_o^2) - z''} \qquad (17)$$

A linear transformation transforms the point L' into point ∞; the circle therefore becomes a straight line. Point $H' = \infty$ becomes point $H'' = 4 + k_o^2$, and the end points C' and D' become the points

$$C'' = 1 + i\,\frac{k_o}{2}(3 + k_o^2)$$

$$D'' = 1 - i\,\frac{k_u(3 + k_o^2)}{2\sqrt{1 + \frac{1}{4}(k_o^2 - k_u^2)}}$$

The treatment thus reduces to the flow of a source and sink at point H'' about the surfaces, illustrated in figure 7. Up to terms of higher order and a real factor, the potential in the vicinity of point $H'' = a_6''$ has the form $\frac{1}{\sqrt{z'' - a_6''}}$. This is easily treated with the Schwarz-Christoffel formula.

3d stage: The outside of polygon A" B" C" D" E" F" G" H" L" is transformed into the upper z-half plane ($y > 0$) (fig. 8). The effect of the approximate method is that the polygon now contains only two angles of magni-

tude $\pi/2$, and three angles of magnitude 2π. The integral following the application of the Schwarz-Christoffel formula therefore lends itself to evaluation without elliptical integrals:

$$z'' = \frac{1}{\omega_1} \int_{a_0}^{z} \frac{(z - a_2)\,(z - a_3)\,(z - a_6)\,dz}{\sqrt{(z - a_1)\,(z - a_4)}\,(z - a_5)^2}$$

ω_1 denotes a scale factor so chosen that point $z'' = 1$ corresponds to point a_1. Owing to the condition that the integral should be real for real $z > a_5 = 0$ (fig. 8), and the further condition that the integral from a_1 to a_4 must be zero, it can even be expressed by an algebraic function:

$$z'' = 1 \pm \frac{1 + \dfrac{a_2\,a_3\,a_6}{a_1\,a_4\,z}}{1 + \dfrac{a_2\,a_3\,a_6}{a_1\,a_4\,a_0}} \sqrt{\frac{a_1 - z}{a_1 - a_0}\,\frac{a_4 - z}{a_4 - a_0}} \qquad (18)$$

Here:

$$a_0 < a_1 \leqq a_2 \leqq a_3 \leqq a_4 < a_5 = 0 < a_6 = 1$$

The prefix of the square root is to be so chosen that the upper half plane $(y > 0)$ is transformed into the z"-plane; real z and $z \leqq a_1$ are to carry the negative prefix, $z \geqq a_4$ the positive sign, while for $a_1 \leqq z \leqq a_4$:

$$z'' = 1 + i\,\frac{1 + \dfrac{a_2\,a_3\,a_6}{a_1\,a_4\,z}}{1 + \dfrac{a_2\,a_3\,a_6}{a_1\,a_4\,a_0}} \sqrt{\frac{z - a_1}{a_1 - a_0}\,\frac{a_4 - z}{a_4 - a_0}} \qquad (18a)$$

Five conditions exist for the parameters a_0, a_1, a_2, a_3, a_4 ($a_5 = 0$, $a_6 = 1$). Two of these follow from the previously cited demands that the transformal function for positive real z must be real, and that the length (C" D") must be equal to the sum of B" C" and D" E":

$$a_2 + a_3 + a_6 = \frac{1}{2}(a_1 + a_4)$$

$$a_1 a_4 (a_2 a_3 + a_3 a_6 + a_6 a_2) = a_2 a_3 a_6 (a_2 + a_3 + a_6)$$

From these equations a_1 and a_4 can be computed. A further deduction is that the function (18) in the points a_2, a_3, a_6 has the desired characteristics, namely, that $\frac{dz''}{dz}$ becomes zero at these points. For this reason, there is no linear term at these points in the power series development for z''; $(z'' - a_i'')$ is proportional to $(z - a_i)^2$. (a_i'' is the image point of a_i; i = 2, 3, 6.)

As the position of points C", D", and H" is defined by the position of C, D, and H in the ζ-plane, the still free parameters a_2, a_3, and a_0 must be so chosen that point C" corresponds to point a_2, point D" to point a_3, and point H" to point $a_6 = 1$. For a_2 and a_3 (which alone occur in the first two conditions), we can restrict ourselves to the range of

$$a_2 < 0; \quad \frac{1}{a_2} \geqq a_3 \geqq -(1 + a_2) - \sqrt{1 + a_2 + a_2^2}$$

The case of the wing without end plates (elliptical lift distribution) is obtained when putting

$$a_1 = a_2 = a_3 = a_4 = -a_6 = -1 \quad (k_o = k_u = 0)$$

while $a_2 a_3 = a_1 a_4 = a_6^2 = 1$ gives the wings with symmetrical end plates ($k_o = k_u$) as computed by F. Nagel (reference 3) by a different method.

IV. THE POTENTIAL

Since our aim in the ζ-plane at a great distance from the section is a flow parallel to the η-axis with a speed w (fig. 5), the development

$$\square(\zeta) = w \frac{b}{2} (-i) \zeta + \ldots . \qquad (19)$$

is valid for the potential $\square(\zeta)$ in the vicinity of $\zeta = \infty$.

The transformal function in the vicinity of $\zeta = \infty$, that is, $z = a_6$ can be represented from equations (16), (17), and (18) in the following form:

$$\zeta = i \frac{M}{z - a_6} (1 + \ldots) = i \frac{M}{z - 1} (1 + \ldots) \qquad (20)$$

Here

$$M = \sqrt{\frac{(3 + k_0^2)(4 + k_0^2)}{C}}$$

and

$$C = \sqrt{\frac{a_6 - a_4}{a_4 - a_0} \frac{a_6 - a_1}{a_1 - a_0}} \frac{C_1}{1 + \frac{a_2 a_3 a_6}{a_0 a_1 a_4}}$$

with

$$C_1 = - \frac{(a_4 - a_1)^2}{8 (a_6 - a_1)^2 (a_6 - a_4)^2} + \frac{a_2 a_3}{a_1 a_4 a_6^2}$$

$$- \frac{a_2 a_3}{a_1 a_4} \left[+ \frac{(a_4 - a_1)^2}{8(a_6 - a_1)^2 (a_6 - a_4)^2} + \frac{2a_6 - (a_1 + a_4)}{2a_6 (a_6 - a_1)(a_6 - a_4)} \right] (a_6 = 1)$$

Then the potential $\square(z)$ has, according to equations (19) and (20), the value:

$$\square(z) = w \frac{b}{2} \frac{M}{z - 1} = \Phi + i \Psi \qquad (21)$$

For real z, $\Psi = 0$, i.e., a doublet with the real axis as a streamline. This result is anticipated (figs. 5 to 8). No further terms occur in the development of $\square(z)$.

Since equations (16), (17), and (18) afforded no simple expression for z as function of ζ, several mathematical examples were computed. First the parameters a_i were determined. Then the correlated image points ζ in the ζ-plane were computed for z values from the interval $a_0 \leqq z \leqq a_{45}$ (point a_{45} corresponds to point F)

with the aid of equations (16), (17), and (18). The pertinent potential $\square(z) = \Phi(z)$ was obtained from equation (20), after which the circulation $\Gamma(\bar{\xi})$ and $\Gamma(\bar{\eta})$, respectively, follows from equation (1).

Note.- The circulation on wings with plates (tail surfaces) of the form of figure 9 can be computed in exactly the same manner. The numerical results are to be published at a future date.

V. NUMERICAL RESULTS

Figure 10 illustrates various circulation distributions $\Gamma(\bar{\xi})$ over the wing and $\Gamma(\bar{\eta})$ over the end plate as obtained with equation (1). It discloses that $\Gamma(\bar{\xi})$ is substantially dependent on the height of the end plates; i.e., on the ratio h/b, and that shifting the point of attachment of the end plate has no material effect on the total circulation. But near to the end plate itself, $\Gamma(\bar{\xi})$ is dependent upon the type of the plate attachment. According to equation (1), Γ is the difference of two potentials. They always proceed at the wing tip with vertical tangent, if the end plate does not protrude on the particular side of the wing; otherwise, the tangent is horizontal. In the first case the flow velocity from pressure toward suction side is infinite at the plate attachment point; in the second case, it is zero. Thus, for an end plate at one tip ($k_o = 0$ or $k_u = 0$), $\Gamma(\bar{\xi})$ has at point $\bar{\xi} = 1$ a vertical tangent; otherwise, the tangent is horizontal.

In figure 11 the value $\kappa = \frac{\pi}{2J}$ (equation 5), that is, the ratio $\frac{c_{w_i}}{c_a^2 \frac{F}{\pi b^2}}$ is shown against k_o for different values of h/b. The total circulation is smallest in the symmetrical case ($k_o = k_u$, $k = 1$), (equation 4), but shifting of the point of attachment of the end plate results in no appreciable change of $\frac{2J}{\pi} = \frac{1}{\kappa}$ (as anticipated from figure 10).

The point of application η_o of the side force S_o at the end plate as well as η_u was determined from equa-

tions (14) and (15). It was found that η_o was approximately proportional to k_o and η_u to k_u.

$$\frac{\eta_o}{k_o} \approx \frac{-\eta_u}{k_u} \approx 0.40 \qquad (22)$$

The value 0.4 is an average value strictly applicable to symmetrical end plates ($k = 1$) only. But the discrepancy (0.39) for all other values, even $k = \infty$, is so small, that 0.40 applies to all k values.

Figure 13 shows the S_o/A ratio against k_o with k and h/b as parameters. The connection between S_o/A and k_o is the same as for S_u/A and k_u, if 1/k is substituted for k in figure 13. In agreement with the fact that wings with end plates at one tip have a total circulation greater than wings with symmetrical end plates, the side force (per unit of length) with end plates at one tip exceeds that of those with symmetrical end plates. Even the quotient S/A (for equal k_o) for end plates at one tip is greater than for symmetrical ones.

The use of unsymmetrical end plates therefore affords an increase in circulation on the wing (and consequently, a lift increase for a certain angle of attack) but only at the expense of considerably greater side forces at the end plate.

To illustrate: For $\frac{h}{b} = 0.3$, a shift of the end plate from symmetrical to one-sided attachment, results in a 2-percent increase in circulation, but the side force on the upper part of the end plate increases almost three times, the arm at which it applies twice, resulting in a moment approximately 500 percent greater.

To simplify the interpolation, we have plotted in figure 14, the ratio c_{s_o}/c_a against k_o with k as parameter. As with k_o, both S_o and F_o approach zero; the ratio c_{s_o}/c_a itself yields finite limiting values for $k_o = 0$. The relation between c_{s_u}/c_a and k_u is the same as between c_{s_o}/c_a and k_o, if k is replaced by 1/k in figure 14. It will be seen that c_{s_o}/c_a can be approx-

imately represented as linear function of k_o for all values of k: $c_{s_o}/c_a = A + B\,k_o$. The A and B constants, being dependent on k, can be defined from figure 14.

According to the foregoing, it is advisable for structural reasons to employ symmetrical end plates. If, of course, the end plates are to serve as controls, then greater horizontal forces are desired. In this case k_u would be chosen as small as possible.

Regarding figures 11 and 13, it should be noted that only the shown points have been computed, after which the curves k = constant and h/b = constant, were obtained by interpolation. This method is well justified in view of the smoothness of the curves.

A comparison of the theory with measurements by O. Schrenk (to be published in the near future), on a wing with end plate at one tip ($k = \infty$; $k_o = 0.092$), is seen in figure 15. The recorded c_a and c_s values are plotted against angle of attack α; c_s was obtained from pressure records (curve D). It also shows the measured values for the moment coefficient of the side force $c_{m_E} = \frac{M_o}{q\,F_o\,h}$ against α, where F_o is the area of the end plate and M_o the moment of the side force S_o about the end plate.

The theoretical c_s values (curve Th.) were computed from the measured c_a values by means of the relation $c_s/c_a = 0.446$ from figure 14. The theoretical curve is in very close agreement with the experimental curve - at least, for positive α. The theoretical moment coefficient c_{m_E} of the side force can be obtained from equation (22):

$$c_{m_E} = \frac{\eta_o}{k_o}\,c_s = 0.4\,c_s$$

which, for the case in point, gives:

$$c_{m_E} = 0.4 \times 0.446\,c_a \quad \text{(curve Th.)}$$

These values are also in very good accord with the values c_{m_E} (curve D) obtained from pressure records.

No better agreement between theory and experiment can be expected, particularly for $c_a = 0$, because the relation $c_s = 0$ following from the theory of infinitely thin flat plate is not fulfilled for $c_a = 0$. This is probably due to the fact that owing to the finite thickness of the profile and of the end plate and the profile camber, even at zero total lift, suction forces occur at certain points which occasion an inwardly directed force at the end plate.

Translation by J. Vanier,
National Advisory Committee
for Aeronautics.

REFERENCES

1. Munk, M. M.: Isoperimetrische Aufgaben aus der Theorie des Fluges. Diss., Gottingen University, 1918.

2. Prandtl, L.: Tragflügeltheorie, I and II, 1918-19.

3. Nagel, F.: Flügel mit seitlichen Scheiben. Vorläufige Mitteilungen der Aerodynamischen Versuchsanstalt zu Gottingen, vol. II, July 1924.

4. Trefftz, E.: Prandtlsche Tragflächen- und Propellertheorie. Z.f.a.M.M., vol. I, 1921, p. 206.

5. Prandtl, L., and Betz, A.: Ergebnisse der Aerodynamischen Versuchsanstalt zu Göttingen, Lfg. III, 1927.

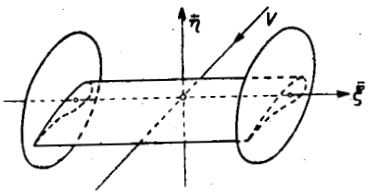

Figure 1.- Wing with end plates.

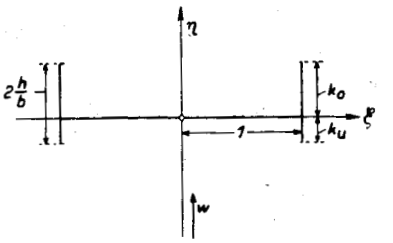

Figure 2.- Section through vortex surface leaving the wing with end plates.

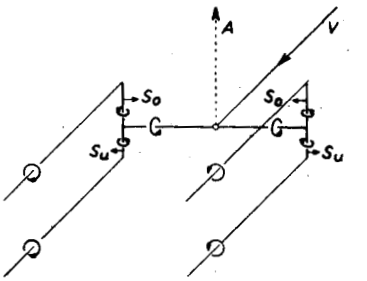

Figure 3.- Bound and free vortices.

Figure 5.- The ζ plane.

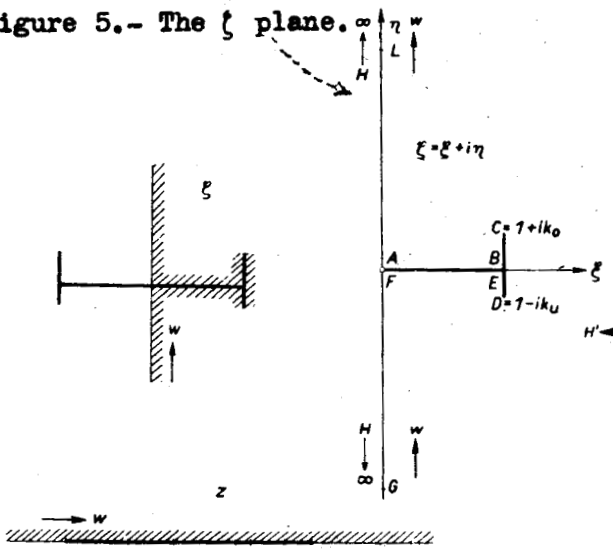

Figure 4.- Conformal transformation of the ζ on the Z plane.

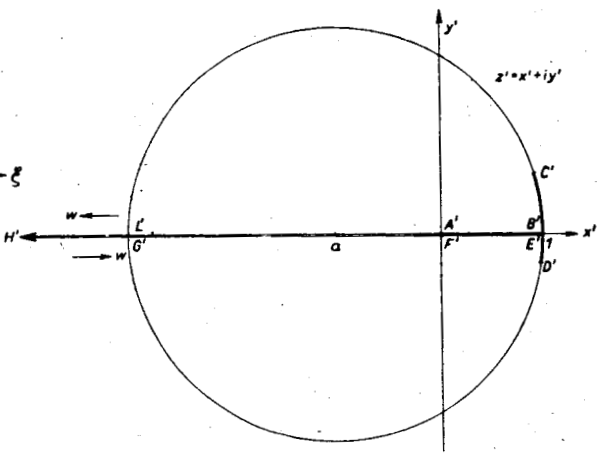

Figure 6.- The Z' plane.

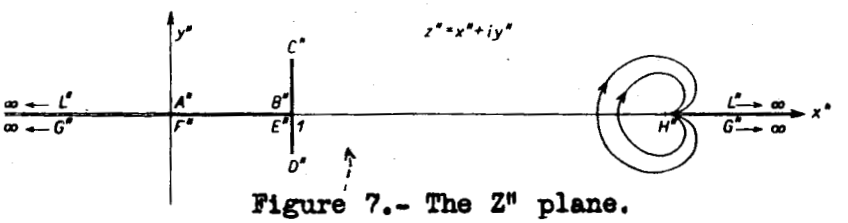

Figure 7.- The Z" plane.

Figure 8.- The Z plane.

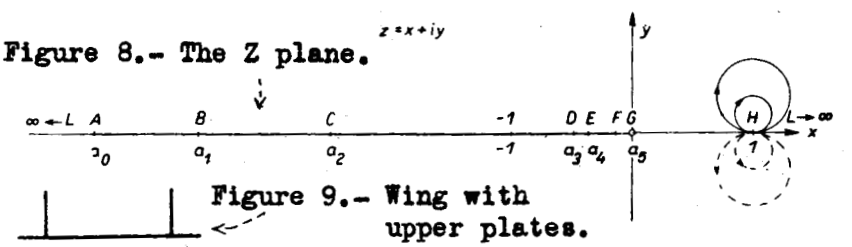

Figure 9.- Wing with upper plates.

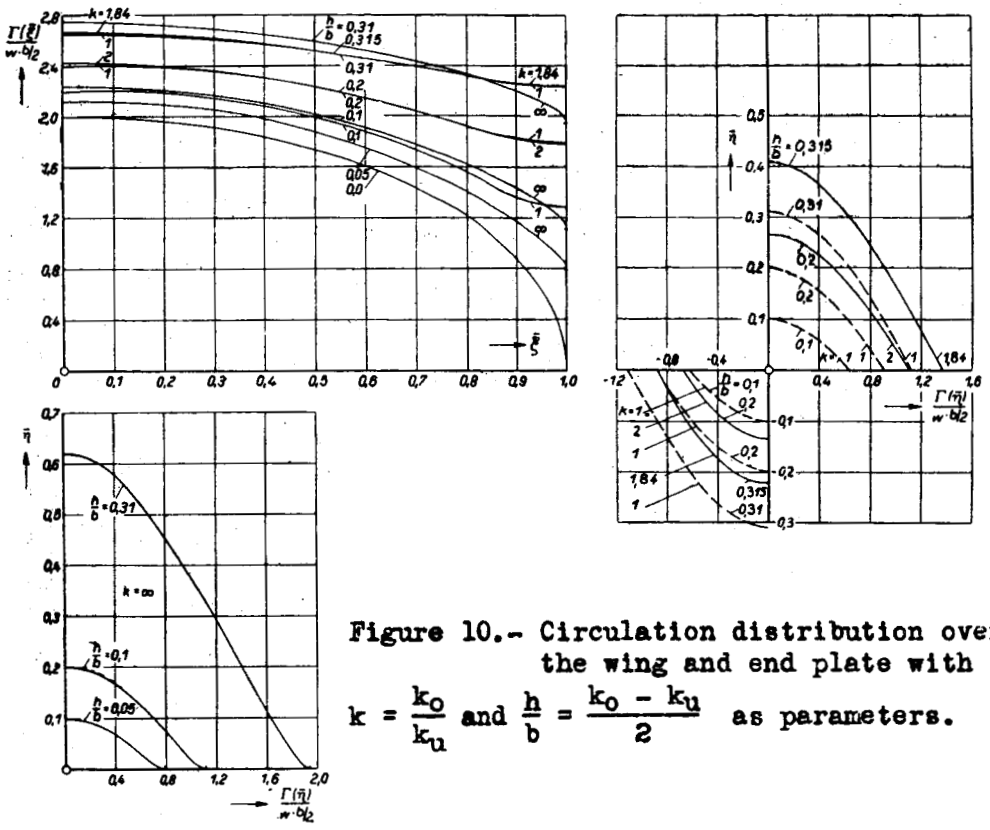

Figure 10.- Circulation distribution over the wing and end plate with $k = \frac{k_o}{k_u}$ and $\frac{h}{b} = \frac{k_o - k_u}{2}$ as parameters.

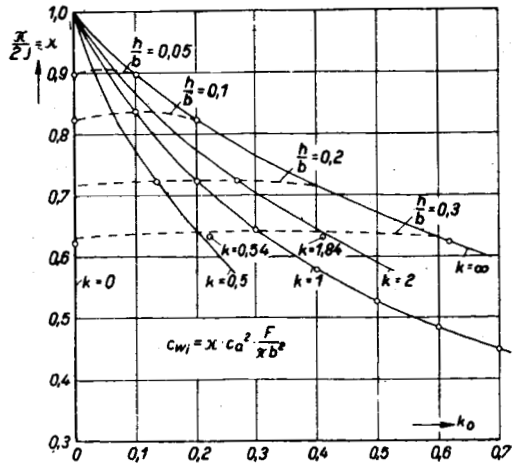

Figure 11.- Induced drag of wings with end plates.

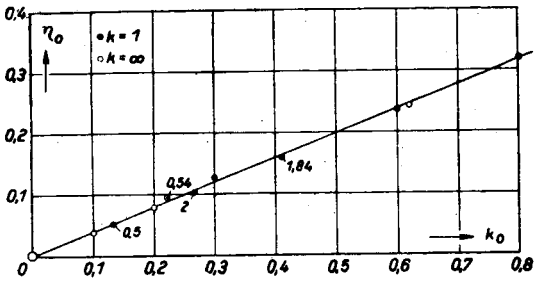

Figure 12.- Point of application of side force against end plate dimensions.

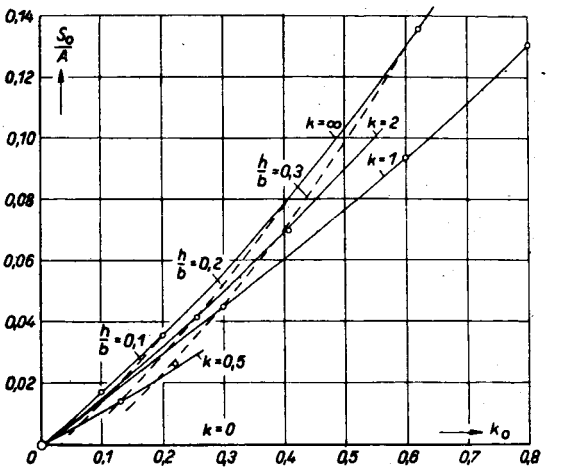

Figure 13.- Side force against length and position of end plate.

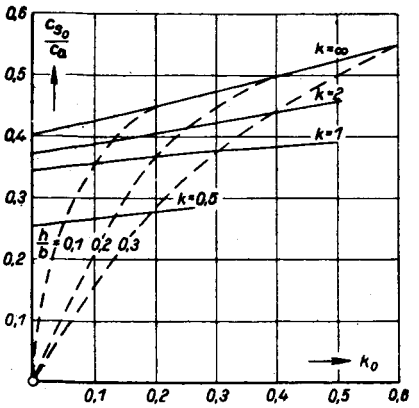

Figure 14.- Ratio c_{so}/c_a against height and position of end plate.

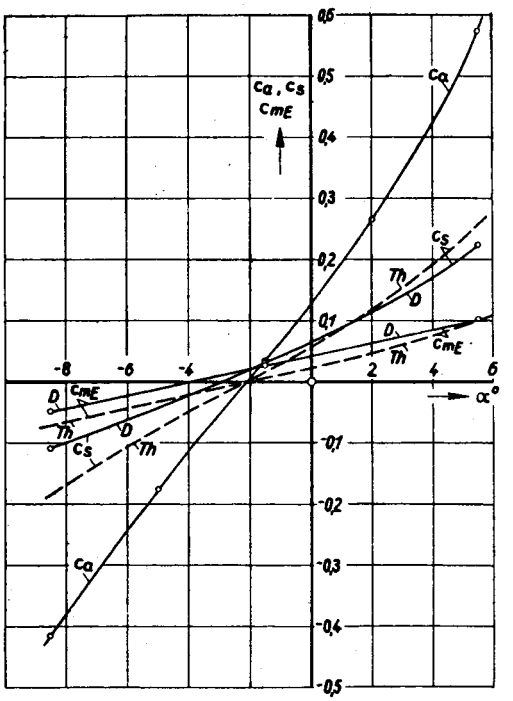

Figure 15.- Theory compared with Schrenk's measurements.